Chapter 13

Tapered Plasmonic Nanoantennas for Energy Harvesting Applications

Youssef Mamdouh El-Toukhy,
Mohamed Farhat Othman Hameed,
Mohamed Hussein and Salah Sabry Ahmed Obayya

Additional information is available at the end of the chapter

http://dx.doi.org/10.5772/67418

Abstract

In this chapter, novel designs of tapered-dipole nanoantennas are investigated for energy harvesting applications. A full systematic analysis for the proposed structure is presented where the harvesting efficiency, return loss, radiation pattern, and near-field enhancement are calculated using a finite-element frequency domain solver. Simulation results show that the proposed nanoantennas can achieve a harvesting efficiency of 60% at a wavelength of 500 nm where the antenna input impedance is matched to that of fabricated rectifying devices. Additionally, the cross-tapered nanoantenna offers a near-field enhancement factor of 252 V/m, which is relatively high compared to previously reported nanoantennas. The spatial and spectral resonance modes are investigated, and the simulation results indicate the ability of the cross geometry to be utilized in color-sorting applications. Moreover, the particle swarm optimization technique is adapted to configure the proposed designs for maximum performance.

Keywords: nanoantenna, energy harvesting, plasmonics, finite-element frequency domain, particle swarm optimization, metal/insulator/metal diode, color-sorter

1. Introduction

The strong electromagnetic field enhancement of metallic plasmonic structures has encouraged the utilization of such devices in various applications. This enhancement is attributed to the plasmonic resonance that occurs at the near-field region of metals such as silver or gold. Plasmonic nanoantennas have gained the main interest, theoretically and experimentally,

among recent researchers in the fields of energy harvesting [1–4], bio-sensing [5], plasmonic nanosensors [6], and optical communications [7]. Similar to plasmonic devices, the high-field confinement of nanoantennas is directly related to the metal refractive index and the design geometry. Other major parameters of the nanoantenna performance are harvesting efficiency, which is the efficiency by which light energy is collected, and the antenna impedance that defines the coupling efficiency between the nanoantenna and other devices.

Due to the large worldwide demand on renewable energy, an intense research work has been directed toward benefiting from the solar energy as a free and clean source. In early 1970s, Bailey has proposed the concept of rectenna in the field of solar energy harvesting [8] where rectenna stands for a rectifying diode coupled with antenna. Nanoantenna is responsible for transforming solar radiation into an alternating current (AC) electric field across the diode, which rectifies the signal to obtain direct current (DC) power. In recent years, rectennas design and fabrication techniques are getting more mature as this approach promises to offer highly efficient solar energy harvesting systems. Referring to the radiation spectrum of the sun, maximum irradiance occurs at the visible wavelength range from 400 to 700 nm. Nonetheless, extending the utilization of rectenna systems to visible frequencies (PHz) resulted in several challenges. First, the challenge of scaling down antenna dimensions to sub-micrometer is becoming more realizable with advanced technologies [1]. A second challenge is the existence of suitable rectifiers for these operation criteria. Metal\insulator\metal (MIM) diode topology is gaining interest as a candidate for high-frequency operation [9]. Additionally, the main factors contributing to the efficiency of nanorectenna systems are (1) harvesting efficiency and field confinement of the nanoantenna device; (2) the cut-off frequency of the diode and responsivity at zero voltage bias; and (3) impedance matching between the nanoantenna and the diode.

Vandenbosch and Ma [10, 11] reported an upper bound for total solar harvesting efficiency of 64%, over wavelength range 400–1200 nm, for a silver-dipole nanoantenna. This design offers a nominal input impedance of 250 Ω at resonance and harvesting efficiency of 26% at wavelength of 500 nm. Bowtie [12, 13] and Vivaldi [14] nanoantennas offered a low input impedance of about 100 Ω at resonance. However, authors study did not provide calculations for harvesting efficiency at visible light range. Other design topologies were proposed, such as spiral, log-periodic [15], flower-shaped dipole, and elliptic dipole nanoantenna [16]. While some of these designs offer higher efficiencies up to 90% at 500 nm wavelength, they suffer from very high design complexity and the lack of impedance analysis in the literature, especially over the visible light region. A tapered-dipole nanoantenna topology was first introduced in Ref. [17] where two structures were presented, two-arm and cross-arm dipole antennas with tapered end. The simulation results for these structures show high-field confinement in the antenna gap where the cross-dipole antenna exhibits the higher field enhancement. However, this study was not intended for solar harvesting application, and thus, no further analysis for the harvesting efficiency or input impedance was presented [17]. A study of the field distribution around nanoantenna and current induced on the surface was also carried out for the bowtie and spiral designs [12, 15] where simulation and experimental results showed high enhancement over the conventional dipole design [11]. However, these rectenna devices suffer from low coupling efficiency between nanoantenna and rectifier due to high impedance mismatch.

Moreover, cross antenna design topology has been previously investigated several times due to its compatibility with special applications such as fluorescence-sensing [17], color-sorting [18, 19], and high-harmonic generation [20]. These applications take advantage of cross antenna electromagnetic characteristics such as dual resonance, high-field confinement, and polarization control. The dual resonance characteristics of the cross antenna topology arise from the four-arm nature of the antenna and the interaction between the incident field with both x- and y-oriented arms. This phenomenon also enables the antenna to interact strongly with both polarization, horizontal and vertical. Additionally, cross nanoantennas have been previously reported to achieve higher field enhancement than the corresponding two-arm structure where Ying-Ying et al. [20] studied the field enhancement of a nanoellipsoid cross antenna which reached slightly below 200 enhancement factor. Another research work reported an enhancement factor of 320 for symmetric cross bowtie nanoantenna, on a fused silica substrate, operating as a color-sorter [19].

This chapter demonstrates two novel nanoantenna designs, which offer harvesting efficiencies up to 60% at wavelength λ of 500 nm with a field enhancement factor about 10 times greater than that of the conventional dipole design. This enhancement is attributed to high divergence of surface current over the nanoantenna surface as a result of the multiple thickness grading introduced to the design. Moreover, both nanoantennas are configured to offer a high-coupling efficiency when connected to a rectifying device by matching the antenna input impedance with that of fabricated MIM diodes operating at THz frequencies. Additionally, the radiation patterns and near-field enhancement factor are presented, which show the high performance of the cross nanoantenna structure over the two-arm dipole design. Furthermore, the near-field intensity spectrum is investigated for both designs, which indicates that the cross-tapered-dipole nanoantenna can be utilized for dual-color sorting applications where it offers a normalized near-field enhancement factor of 252 V/m. All nanoantenna designs are optimized using particle swarm optimization algorithm [21] connected to an electromagnetic solver software.

2. Design consideration

This research work focuses on overcoming the drawbacks of previously studied nanoantenna designs such as low field confinement at the gap, small nominal input impedance, and low harvesting efficiency at visible light frequencies. Moreover, this study introduces a novel design that offers relatively high manufacture feasibility as will be discussed later. For an efficient operation of rectenna system, high-intensity field should exist at the surface of the MIM diode δ_s so that sufficient electrons can tunnel through the diode. Therefore, high-field confinement at the gap of the nanoantenna represents a major requirement in the nanoantenna design. According to electromagnetic theory, electric field tends to be accumulated at the metal tips of the antenna structure [12, 22]. Based on this phenomenon, the proposed design was constructed by inserting more steps of smaller dimensions into the conventional dipole design, as shown in **Figure 1b**, which increases the number of tips and consequently the electric field confinement by the nanoantenna. This is directly related to the antenna efficiency where the harvested electric energy

is transformed to AC power at the antenna port. **Figure 1** demonstrates the design parameters of the conventional dipole and the proposed tapered-dipole nanoantenna, which is considered a modified version of the conventional dipole where two more steps of smaller dimensions are inserted. Additionally, the cross structure of the same nanoantenna is investigated where the four arms of the antenna are placed in the x and y directions, horizontal and vertical orientations, as shown in **Figure 1c**. Silver material is selected for all the nanoantennas studied in this work as it is reported to offer higher efficiency when compared to other metals [11]. The proposed design parameters are chosen using particle swarm optimization (PSO) technique [21] where efficiency, impedance, and/or field enhancement are optimized. The optimization process is carried out through an external link between the algorithm and the finite-element frequency domain (FEFD) solver [23]. The PSO technique will be discussed in the next section. Additionally, a minimum feature size of 5 nm is maintained in grading adjacent dipole steps to reduce design complexity.

The suggested designs can be fabricated using top-down methods such as electron-beam lithography (EBL) and focused ion beam (FIB) techniques [14]. The EBL is employed to define desired patterns down to the nanometer scale in resists. Therefore, it is normally combined with stripping (lift-off) or etching to obtain the desired patterns in the target materials. For a specific EBL technique, reported in Ref. [24], 4–8 nm patterning and lift-off were achieved for Au nanoparticles. On contrast to EBL, the FIB technique can define patterns down to the nanoscale without using masks [25]. Most widespread instruments of FIB use gallium ion source, which is capable of fabricating sub-5 nm holes [26]. Another technique of FIB is called Helium ion beam milling, which is inherently less damaging to the sample than Ga ions but ideal for structuring thin slabs of material with high precision [27]. The helium milling was reported to achieve 5–10 nm resolution in patterning a thin gold film using milling from sides to center [27]. These fabrication methods have been commonly used in manufacturing nanoantennas with highly controllable parameters. However, the fabrication of several nanoantenna structures (such as bowtie [13], spiral [15], elliptical, and flower [16])

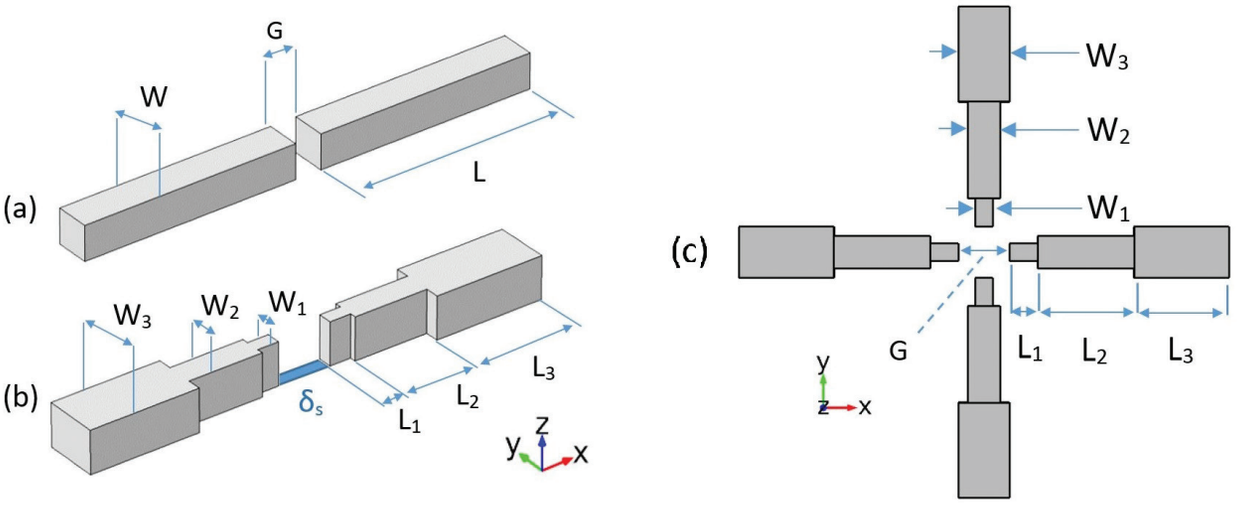

Figure 1. The schematic design of (a) conventional dipole nanoantenna [10], (b) tapered dipole nanoantenna [3], and (c) cross-tapered dipole nanoantenna.

suffers from the complexity of the lift-off process for ultra-small features and curvatures since resists are difficult to strip away. The proposed design offers high feasibility since it does not include sharp tips or curvature. Furthermore, tapered dipole and cross structures have a minimum feature size of 5 nm to be compatible with the techniques stated above and a large gap size to facilitate the fabrication process [14].

3. Particle swarm optimization

The relatively fast and accurate simulation of nanostructures operating at TeraHertz frequencies has created a space for stochastic optimizers to participate in design process refinement for various engineering electromagnetic (EM) problems where a link between the optimization algorithm and the EM solver is created. Particle swarm optimization (PSO) was previously introduced to the nanoantenna field [28] and has a great potential in the microwave antenna design recently by the authors [29, 30]. Kennedy and Eberhart were the first to introduce the PSO concept [21]. Since its creation in 1995, PSO has been reported as one of the highly efficient optimizing technique for solving complicated optimization problems even when compared to other techniques like genetic algorithms (GAs) or differential evolution [31, 32]. The PSO technique is inspired by the behavior of birds or fish, looking for food, which shows social and cooperative approach. Furthermore, for a certain EM problem, the solution is defined by N dimensions, which correspond to the design parameters to be optimized. The optimization algorithm employs the swarm intelligence to search for the optimum solution at which single or multiple performance-based parameters are maximized; in some cases, minimum value is required. These parameters are calculated by the external EM solver, which acts as fitness function evaluator; then, values are sent back to the PSO algorithm for processing.

The PSO algorithm consists of the initialization for a population (swarm) of candidate solutions called particles. The algorithm spreads these particles in the search domain, which resembles the solution space, with a prespecified velocity to find the optimal solution. Each particle possesses a memory, which is used to keep track of its previous best position. Two positions are defined after each iteration, which is the personal best position (Pbest) and the global best position (Gbest) of the whole swarm. The next step is to update the positions and velocities of the swarm particles, which represent the core of all stochastic optimization algorithms. The Gbest swarm topology [30] is utilized where Pbest is updated based on the latest fitness function value, and Gbest is obtained by sharing all known Pbest locations with the rest of the swarm and choose the location which corresponds to optimum value of the fitness function. The flow chart of the adopted PSO algorithm is shown in **Figure 2**.

At the nth iteration, the particle velocities and positions are updated by:

$$v_n = \omega * v_{n-1} + c_1 * r_1 * \left(Pbset_{n-1} - x_{n-1}\right) + c_2 * r_2 * \left(Gbset_{n-1} - x_{n-1}\right) \quad (1)$$

$$X_n = X_{n-1} + v_n \quad (2)$$

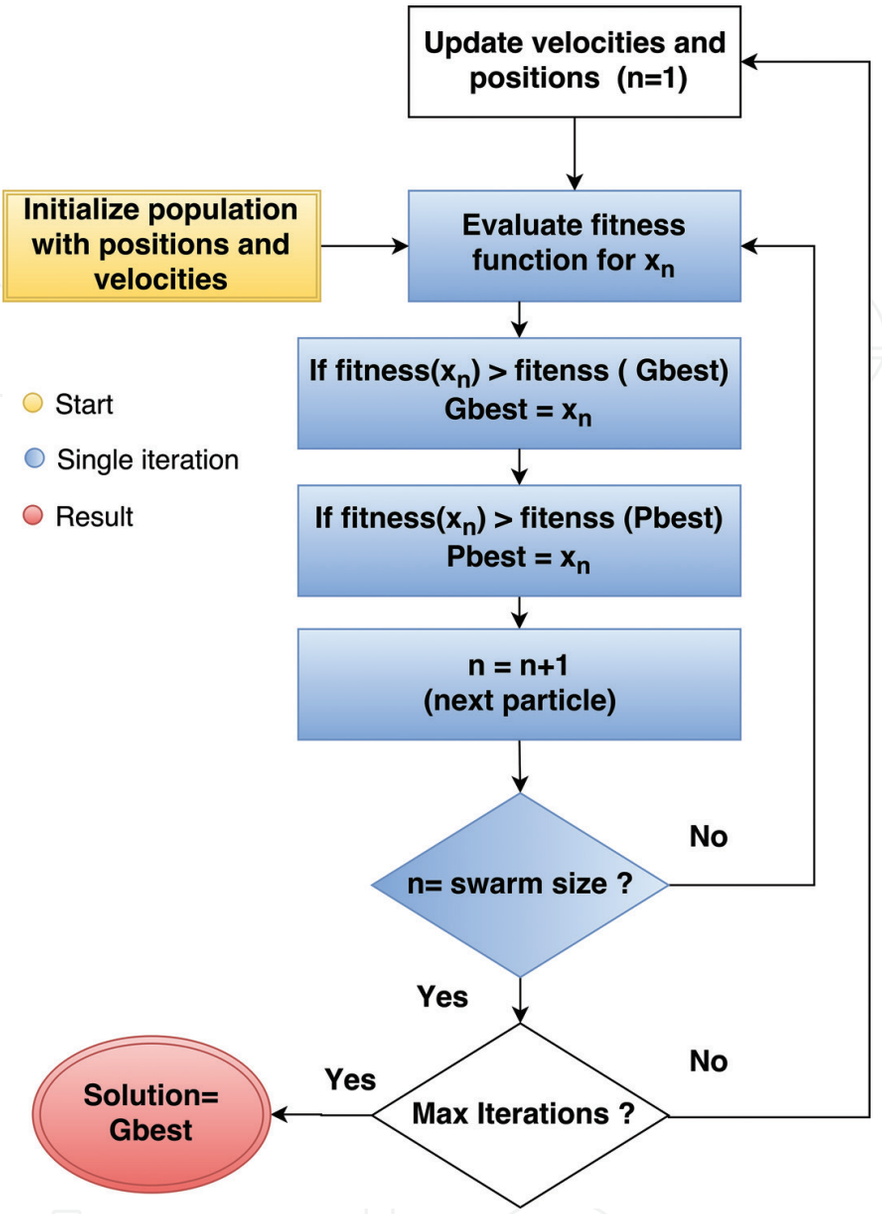

Figure 2. The flowchart of the PSO algorithm.

where r_1 and r_2 represent random numbers between 0.0 and 1.0. These random elements are introduced into the optimizer to simulate the slight unpredictable component of natural swarm behavior. Further, ω is the inertial weight, which keeps each particle in its current trajectory.

4. Simulation methodology

The proposed nanoantenna designs are analyzed using FEFD method via Comsol Multiphysics software [23] where the harvesting efficiency, return loss, and input impedance are calculated at a wavelength of 500 nm. The constructed model uses a fine mesh with a minimum and maximum element sizes of 1 and 10 nm, respectively, to resolve the skin depth of silver (3 nm

at 500 nm wavelength). The studied nanoantennas have a fixed thickness T of 40 nm, indicated in **Figure 1**, and are surrounded by free space everywhere as in Refs. [10, 33]. The boundary conditions are set to perfect matched layer (PML), and the permittivity of silver introduced in the model is taken from Johnson and Christy [34]. According to the reciprocity theorem, the efficiency of an antenna in the transmission mode η_{rad} is equal to the efficiency in receiving mode. The radiation efficiency of an antenna is calculated as [10]:

$$\eta_{\text{rad}} = \frac{P_{\text{rad}}}{P_{\text{in}}} = \frac{P_{\text{rad}}}{P_{\text{rad}} + P_{\text{loss}}} \tag{3}$$

where P_{rad} is the total radiated power, P_{in} is the power input at the antenna port, and P_{loss} represents the power dissipated in the nanoantenna material. **Table 1** shows the equations used to calculate P_{rad} and P_{loss} where S_{sc} is the scattered intensity pointing vector, J is the antenna surface current, and Q_{rl} together with Q_{ml} represent the resistive losses and magnetic losses, respectively.

$P_{rad} = \oiint S_{sc}\, ds$	$P_{\text{loss}} = \iiint_{\text{antenna volume}} Q\, dV$
$S_{sc} = \frac{1}{2} Re(E \times H^*)$	$Q = Q_{rl} + Q_{ml}$
$Q_{rl} = \frac{1}{2} Re(J \,.\, E^*)$	$Q_{\text{ml}} = \frac{1}{2} Re(j\omega B \,.\, H^*)$

Table 1. Radiated power and power loss equations extracted from the simulated electric and magnetic fields [23, 35].

5. Results and discussion

5.1. Harvesting efficiency analysis

In this analysis, the dipole nanoantenna is excited at its gap by a voltage imposed between the two conducting arms of the dipole and thus corresponds to Thevenin equivalent circuit. This approach, also known as gap excitation, is previously reported to result in antenna impedance very similar to that calculated using conventional feeding line excitation [21]. A nominal diode impedance of 500 Ω was chosen, which corresponds to the fabricated MIM diode reported in Ref. [9]. This diode impedance acts as the Thevenin impedance of the source feeding the nanoantenna at the gap. Additionally, this analysis is carried out at λ of 500 nm where the maximum irradiance of the sun occurs. Further, to simulate the cross nanoantenna, the y-oriented and the x-oriented dipoles are shifted away from each other vertically, in z-direction, for a few nanometers so that ports could be defined in the FEFD solver. This method has been previously reported not to affect the harvesting efficiency calculations [36].

Tapered-dipole and cross nanoantennas are optimized to have resonance at λ = 500 nm with an input impedance of 500 Ω to match the diode impedance introduced to the model. The optimization process follows the PSO algorithm to maximize the specific fitness function defined by:

$$f = c_1 \times \eta_{\text{rad}} + c_2 \times \left| S_{11} \right| \tag{4}$$

where S_{11} represents a measure of the reflected power at the antenna port, which is directly related to the antenna impedance. The S_{11} is calculated in dB and has typical values of several decades in negative. Further, η_{rad} is the ratio presented in Eq. (3) and it is less than unity in magnitude. Additionally, c1 and c2 are constants that are chosen as weighting factors to compensate the magnitude variation between S_{11} and η_{rad} so that both parameters have the same influence on the fitness function. Consequently, the optimization process is not carried away by a single parameter value. These constants are chosen through an iterative process where the optimization algorithm is executed repeatedly then c1 and c2 values are adjusted after each iteration in order to optimize both S_{11} and η_{rad} fairly using the PSO algorithm. In both cases of nanoantennas, the optimizer works through a seven − dimensional solution space which resembles the structure metrics (L_1, W_1, L_2, W_2, L_3, W_3, G). Regarding the optimization of tapered-dipole nanoantenna design, the PSO algorithm converged to maximum value of fitness function in about 100 iterations. This is illustrated in **Figure 3** along with the corresponding values of S_{11} and η_{rad} at four points, which show the effectiveness of applying PSO technique in nanoantenna design problems.

For each candidate design, some constraints must be present in order to pass the values to the FEFD solver. These constraints are described as:

$$1.\ W_{i+1} > W_i \tag{5}$$

$$2.\ W_{i+1} - W_i > 5\ nm \tag{6}$$

$$3.\ \sum_n L_i \times W_i \leq const, n = 1, 2, 3 \tag{7}$$

$$4.\ G > W_1 \tag{8}$$

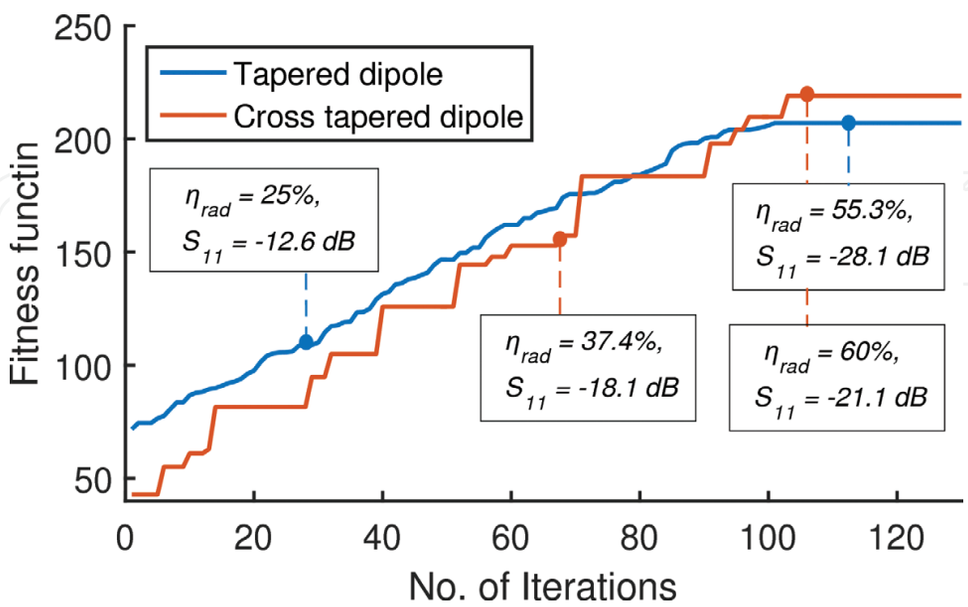

Figure 3. Fitness function (Eq. (4)) values for tapered dipole [3] and cross nanoantenna versus number of iterations of the PSO algorithm. The corresponding values of S_{11} and η_{rad} are demonstrated for four points.

where the first constraint ensures that the confinement occurs at the gap, while the second is introduced to increase design feasibility and reduces manufacture cost. Furthermore, third condition provides that optimized designs do not have exaggerated overall volume where the constant value in the equation represents a measure of the volume of the conventional dipole design in Ref. [10]. The final constraint is only applied in the cross-dipole optimization to prevent adjacent antenna arms from overlapping, which will result in a mathematical error in the FEFD solver.

The optimized nanoantenna dimensions, introduced to the FEFD analyzer, are given in **Table 2** along with the dimensions of the dipole reported in Ref. [10]. The proposed designs show high enhancement over the conventional dipole design, whereas tapered-dipole design achieves $\eta_{rad} = 55.3$ % and $S_{11} = -28.1\ dB$ while the cross-dipole design offers $\eta_{rad} = 60$ % and $S_{11} = -21.1\ dB$ at the same wavelength. On the other hand, the conventional dipole [4] design offers $\eta_{rad} = 26$ % and a near-zero value of return loss at $\lambda = 500$ nm. This is clearly illustrated in **Figures 4** and **5** where the harvesting efficiency and return loss of the tapered-dipole designs are put in comparison with that of the conventional dipole. This enhancement is the result of the multiple tips created in the nanoantenna design, which increases the field accumulation around the antenna structure. On the other hand, the cross-tapered nanoantenna shows a slight increase in the harvesting efficiency, 5% increase. That is due to the increase in the metallic losses of the proposed cross antenna, electric and magnetic, since its volume is almost double that of the two-arm dipole antenna. Additionally, **Figure 6** shows the far-field radiation pattern for both structures, and it is shown from **Figure 6** that cross-dipole nanoantenna obtains a higher gain and a directivity in both x and y directions. This specific characteristic of the cross antenna design can be utilized in optical wireless communication [7].

Additionally, total harvesting efficiency calculations are performed for the proposed nanoantenna designs to obtain a measure of the ultimate optical efficiency over the total wavelength range of the sun irradiance. The total harvesting efficiency can be defined as [10]:

$$\eta_{\text{total}} = \frac{\int_0^{\infty} P(\lambda, T) \times \eta_{\text{rad}}(\lambda)\, d\lambda}{\int_0^{\infty} P(\lambda, T)\, d\lambda} \tag{9}$$

Antenna parameters	Conventional dipole (nm)	Tapered dipole (nm)	Cross-tapered dipole (nm)
T	40	40	40
G	10	49.8	38
L_1	250	5	7.5
W_1	40	13.4	11.5
L_2	–	70	100
W_2	–	19.5	17
L_3	–	103.5	104.4
W_3	–	51	59.6

Table 2. Deign dimensions for the proposed nanoantennas and the conventional dipole [10] for harvesting efficiency analysis.

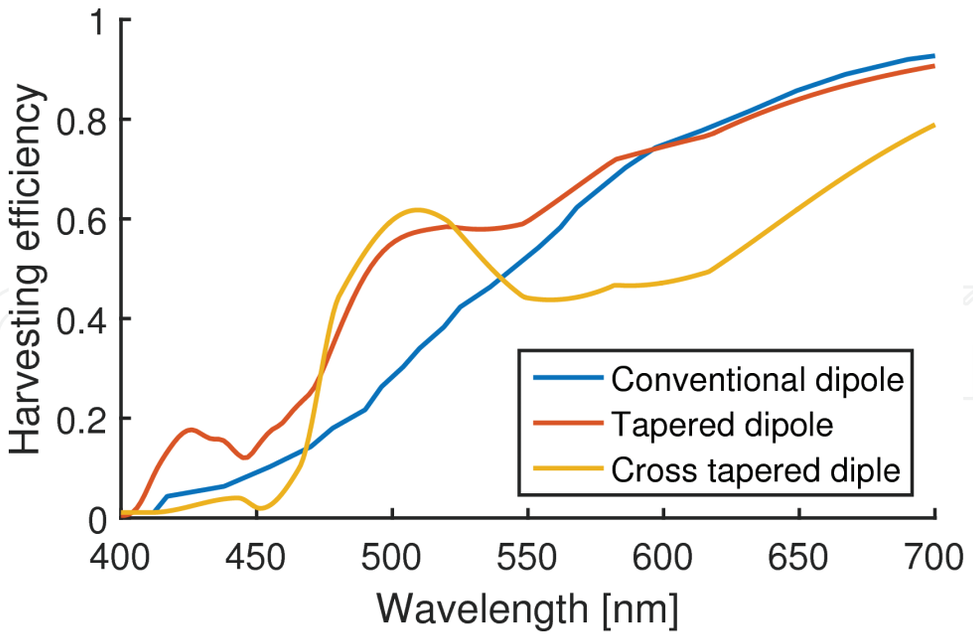

Figure 4. Harvesting efficiency versus wavelength for the conventional dipole [10], tapered dipole [3], and cross-tapered dipole nanoantennas.

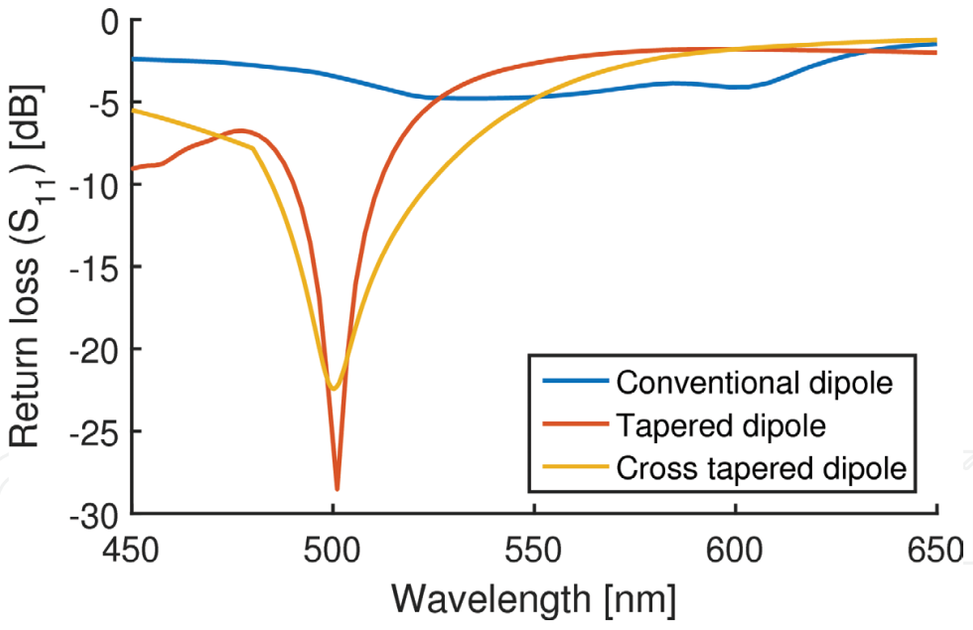

Figure 5. Wavelength dependent return loss at the nanoantenna port for conventional dipole [10], tapered dipole [3], and cross-tapered dipole nanoantennas.

where λ is the wavelength, T is the absolute temperature of the black body (in K), and P is the Planck's law for black body radiation defined in [10]. The total harvesting efficiency values for conventional dipole, tapered-dipole, and cross-tapered-dipole nanoantennas are equal to 64.1, 79.2, and 69.4%, respectively. It is worth noting that the aim of our study is to improve the nanoantenna operation at single wavelength (λ = 500 nm) where the input impedance and

http://dx.doi.org/10.5772/67418

field confinement are optimized. However, calculating the total harvesting efficiency for the proposed design ensures a highly efficient operation at other wavelengths.

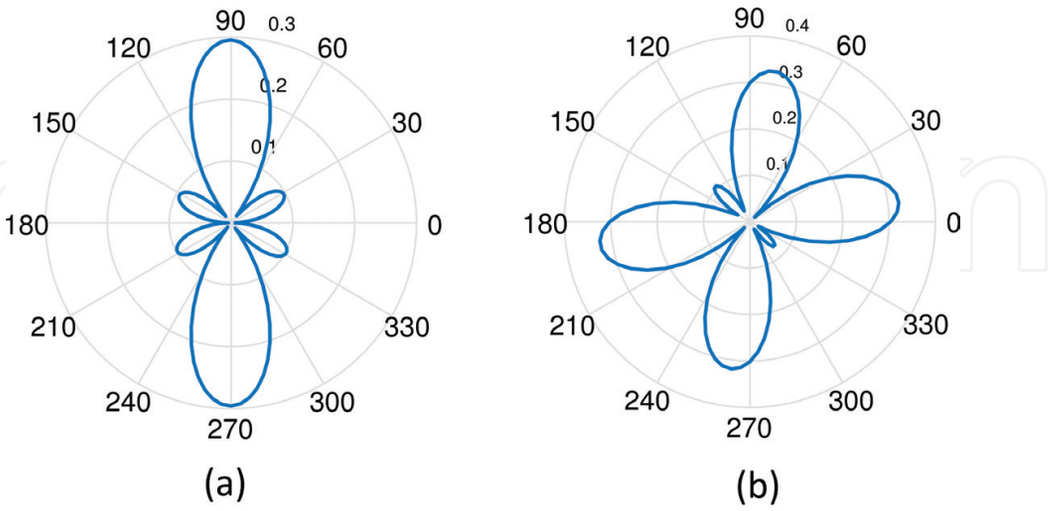

Figure 6. Far-field radiation pattern for (a) tapered dipole nanoantenna and (b) cross-tapered dipole nanoantenna.

To obtain the electric field profile of the studied nanoantenna designs, the whole structure is illuminated by a normally incident plane wave. The incident electric field has an intensity of 1 V/m and a linear polarization where, for the conventional and tapered dipole, the polarization is parallel to the antenna axis (x-axis). As for the cross-tapered-dipole nanoantenna, two polarization settings are studied, x- and y-polarization. The nanoantenna design dimensions are listed in **Table 2** as in the previous analysis. However, the gap size is held constant during this investigation at 10 nm for all design topologies due to its major effect on the field confinement through the gap. **Figure 7** illustrates the electric field profile for conventional dipole and tapered-dipole nanoantennas at $\lambda = 500$ nm. Additionally, the field profiles of the cross antenna structure are demonstrated in **Figure 8a** and **b**, which resemble x-polarized and y-polarized illuminations, respectively. As demonstrated in these figures, the electric field is accumulated with high intensity around the tips of the three nanoantennas, where a high divergence of surface current occurs [12], while the cross nanoantenna topology produces the maximum field confinement in the gap. To have a measure for this improvement, the electric field enhancement factor is calculated for the three nanoantenna structures where this factor corresponds to the maximum normalized electric field within a plane that cuts through the center of the antenna thickness [19]. As a result, the enhancement factors for the conventional dipole, tapered-dipole, and the cross-tapered-dipole nanoantennas are 12.7, 33, and 114 V/m, respectively. This high near-field intensity of the cross geometry is attributed to the field coupling between the four arms of the cross antenna structure which results in higher field confinement in the antenna gap. Another major advantage of the cross antenna structure is that it can interact efficiently with all types of polarization [19], as shown in **Figure 8**. On the contrary, two-arm dipole structures only allow for interaction with single orientation of the electric field polarization, which is parallel to the antenna axis.

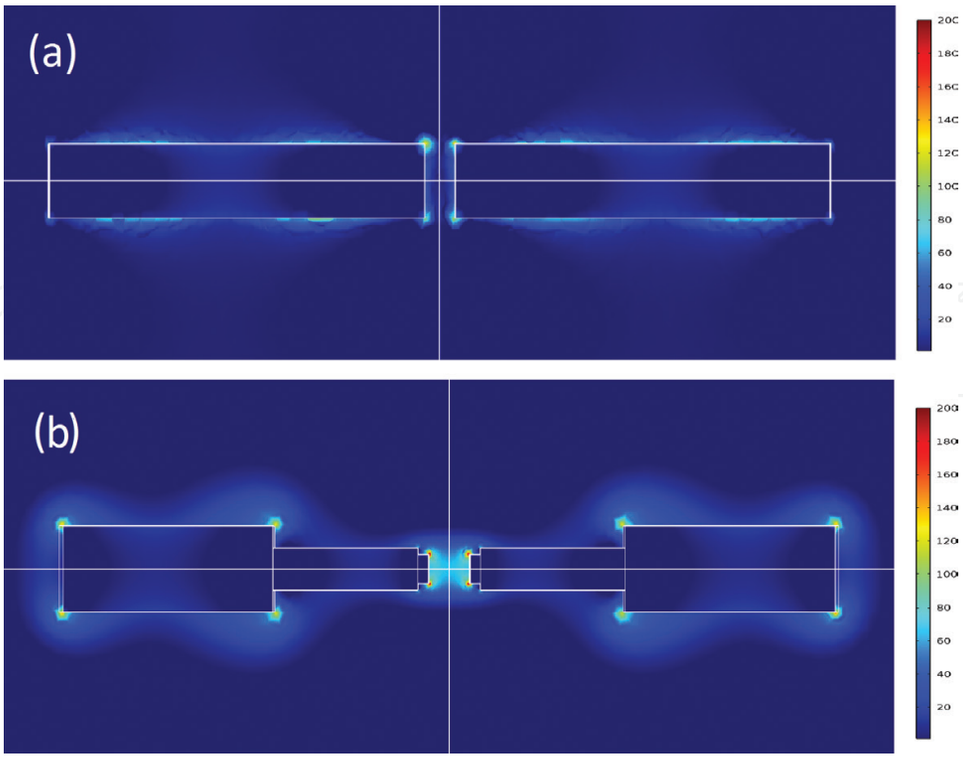

Figure 7. Electric field profile for the (a) conventional tapered dipole [10] and (b) the tapered dipole design [3].

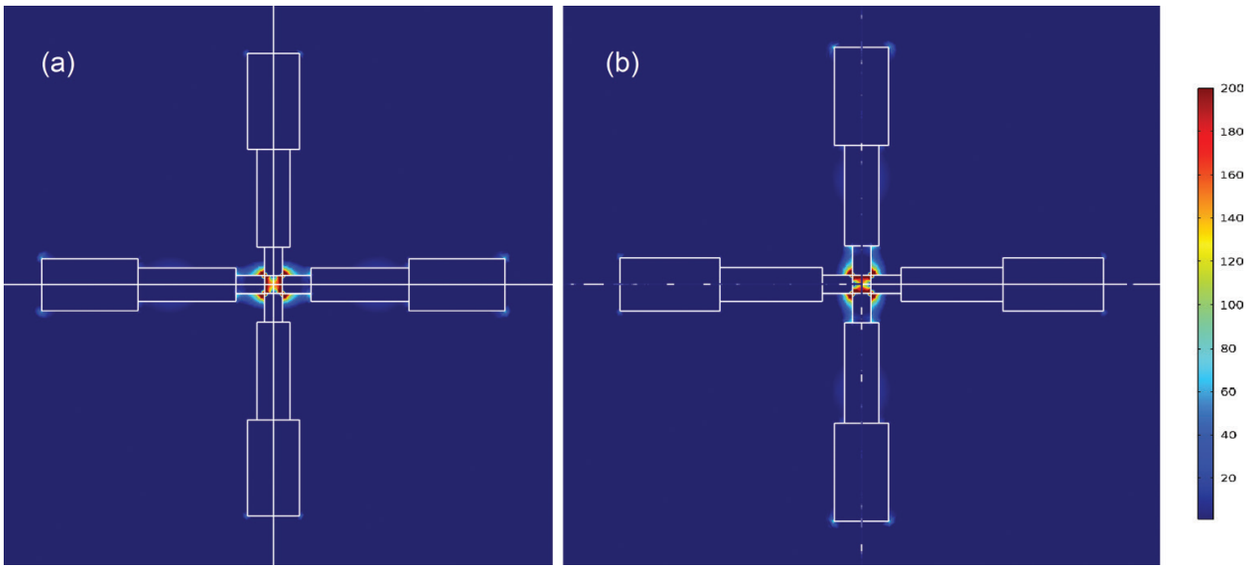

Figure 8. Electric field profile for the cross-tapered dipole nanoantenna for incident wave with polarization in (a) x-direction and (b) y-direction.

5.2. Near-field intensity spectrum analysis

In this study, the near-field intensity enhancement is investigated for the two-arm and cross-tapered-dipole nanoantennas over the range of visible wavelengths from 400 to 700 nm. The constructed model for the two antenna structures follows the same FEFD technique, meshing sizes, and boundary conditions. However, both structures are illuminated

http://dx.doi.org/10.5772/67418

with an x-polarized electric field with amplitude of 1 V/m [19], and the permittivity of silver material is extracted from Ref. [37]. The tapered dipole and the cross-tapered dipole nanoantennas are optimized to achieve maximum near-field intensity over the visible light spectrum. Therefore, the optimization algorithm's fitness function is changed to equal to the field enhancement factor defined in the previous section. The optimized dimensions of the two-arm and cross-tapered dipole are listed in **Table 3**. It can be concluded from the optimization results, stated in **Table 3**, that maximum field enhancement occurs at the lowest values of the antenna gap. This inverse proportionality was previously reported in several studies where it was attributed to the increase of electromagnetic coupling between the metallic antenna elements as the gap size decreases [12, 19]. At this point, it is essential to notice that the optimization algorithm, in the previous section, was targeting an input impedance of 500 Ω for the two optimized nanoantenna structures in order to minimize the coupling losses for further integration with a rectifying diode. Therefore, the sizes of the antennas' gap reached values that are relatively large when compared to the gap sizes for maximum near-field intensity. This can be explained in the context of the effect of the gap size on the antenna input impedance where it was reported that the radiation resistance is directly proportional to the total electrical length of the antenna, which Is a function of total length, diameter, and gap size [37, 38]. Moreover, this study explores the utilization of the proposed nanoantenna structure to other field of applications, such as color-sorter and fluorescence-sensing [17–19].

When a dipole nanoantenna is illuminated with linearly polarized electric field, parallel to its axis, a primary plasmonic resonance occurs in the metallic nanoantenna, which is known as dipole mode [39, 40]. This dipole mode corresponds to a peak value of the near-field intensity at the resonance wavelength. **Figure 9a** shows the normalized near-field intensities for the optimized two-arm–tapered dipole, listed in **Table 2**, which indicates a maximum intensity of 51 V/m at a wavelength of 505 nm. Additionally, the field intensity distribution at the resonance wavelength, 505 nm, is presented in **Figure 9b**, which encounters a very strong electric field at the antenna gap and lower intensity at the edges of the nanoantenna outside stubs. The case is different when investigating the near-field intensity for the cross-tapered-dipole structure. Although a primary dipole plasmonic mode is excited, as in the two-arm dipole, another higher order mode exists at a second resonance wavelength [19]. This can be clearly illustrated by the

Antenna parameters	Tapered dipole (nm)	Cross-tapered dipole (nm)
T	40	40
G	5.3	18
L_1	31.3	27.6
W_1	5	17
L_2	100	94.5
W_2	15	31.8
L_3	91	92.7
W_3	60	50

Table 3. Deign dimensions for the proposed nanoantenna and the conventional dipole [10] for near-field spectrum analysis.

near-field intensity spectrum shown in **Figure 10**. It is evident from **Figure 10** that an intensity peak exists at the primary resonance wavelength of 530 nm, which resembles the dipolar mode, and a weaker blue-shifted shoulder is also present at a wavelength of 425 nm. This can be attributed to the split of the individual dipole mode into two discrete modes, which breaks the single-intensity peak into two distinct resonant peaks [40]. The values of the near-field intensity at the first and second resonance frequencies are 86 and 252 V/m, respectively, which is higher than that of the previously reported nanoantenna in the visible light region [20]. Moreover, the dual resonance characteristic of the cross nanoantenna structure allows it to be employed in fluorescence-sensing applications where the nanoantenna can be optimized to have two resonance wavelengths that correspond to the pump and emission wavelengths at shorter and longer wavelengths, respectively [17]. Consequently, a fluorescent molecule, that is coupled with the cross nanoantenna, is expected to have an enhanced emission [17].

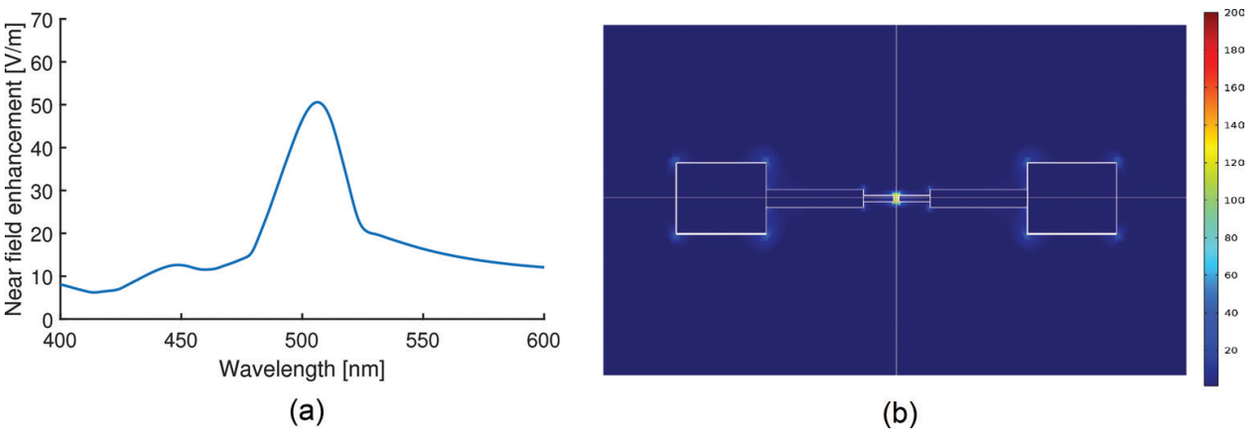

Figure 9. (a) Near-field intensity spectrum and (b) electric field profile for the optimized tapered dipole nanoantenna.

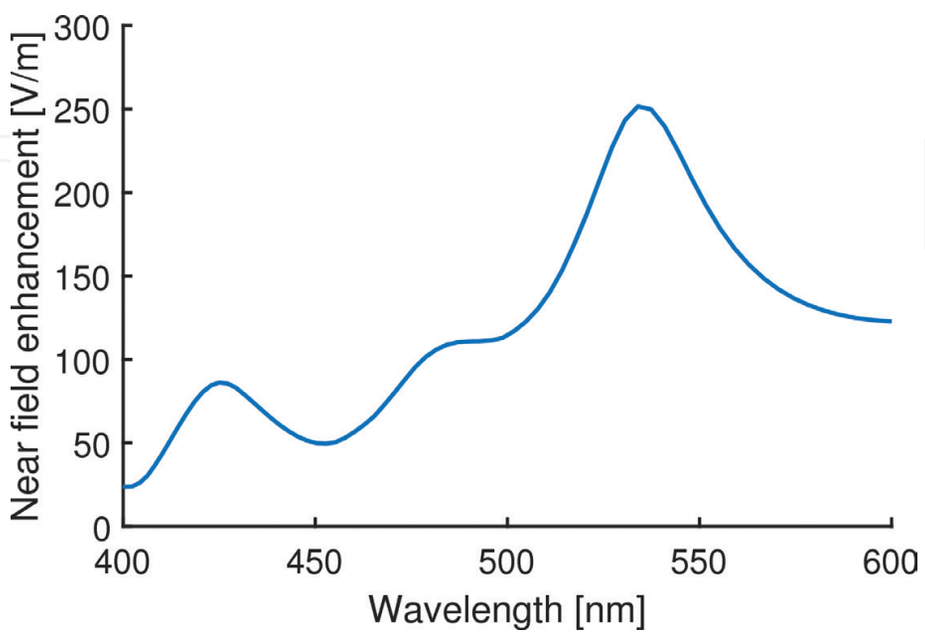

Figure 10. Near-field intensity spectrum for cross-tapered dipole nanoantenna.

Furthermore, a study of the spatial aspect of the two resonance modes of the cross nanoantenna is carried out where the field profiles associated with the two resonance wavelengths are plotted in **Figure 11**. It may be seen from **Figure 11** that the two resonant modes have totally different spatial field distributions. This can be explained through the interaction of the incident electric field with the x-oriented and y-oriented arms of the cross-tapered dipole nanoantenna. **Figure 11a** indicates that the shorter wavelength mode results from the interaction between the incident field and the y-oriented dipole of the cross antenna where the longer resonance wavelength originates from the x-oriented dipole, which is parallel to the polarization axis of the incident wave, **Figure 11b**. As a result, the proposed cross-tapered-dipole nanoantenna can be classified as a color-sorter device [19]. This class of devices is designed to control the spatial distribution of light's different wavelengths at the nanoscale. Therefore, nano-color-sorters are used to filter and steer specific spectral components of light which can be used in various applications such as ultrafast wavelength-selective photo-detection and surface-enhanced Raman spectroscopy [18]. For the specific cross-antenna dimensions, studied here, the tapered-dipole cross nanoantenna can be used to filter 425 and 530 nm wavelengths, which corresponds to violet and green colors. Moreover, the proposed nanoantenna can be optimized to filter almost any two wavelengths as it possesses many degrees of freedom, corresponding to the widths and lengths of each dipole step. Additionally, color-sorter device performance can be enhanced through the introduction of asymmetry into the nanoantenna design [19, 20, 41].

5.3. Fabrication tolerance for tapered dipole nanoantenna

While modern techniques are available for fabricating nanoantenna devices, fabrication processes at nanoscale always convey some perturbation. Therefore, a study of the fabrication tolerance is performed for tapered-dipole nanoantenna structure. This study is directed to calculate the sensitivity of the nanoantenna performance while introducing minor changes to the structure dimensions (L_1, W_1, L_2, W_2, L_3, W_3). It is worth noting that the tolerance of a specific parameter is studied while other parameters of the design are held constant at their optimum values (L_1 = 103.5 nm, W_1 = 51 nm, L_2 = 70 nm, W_2 = 19.5 nm, L_3 = 5 nm, W_3 = 13.4 nm).

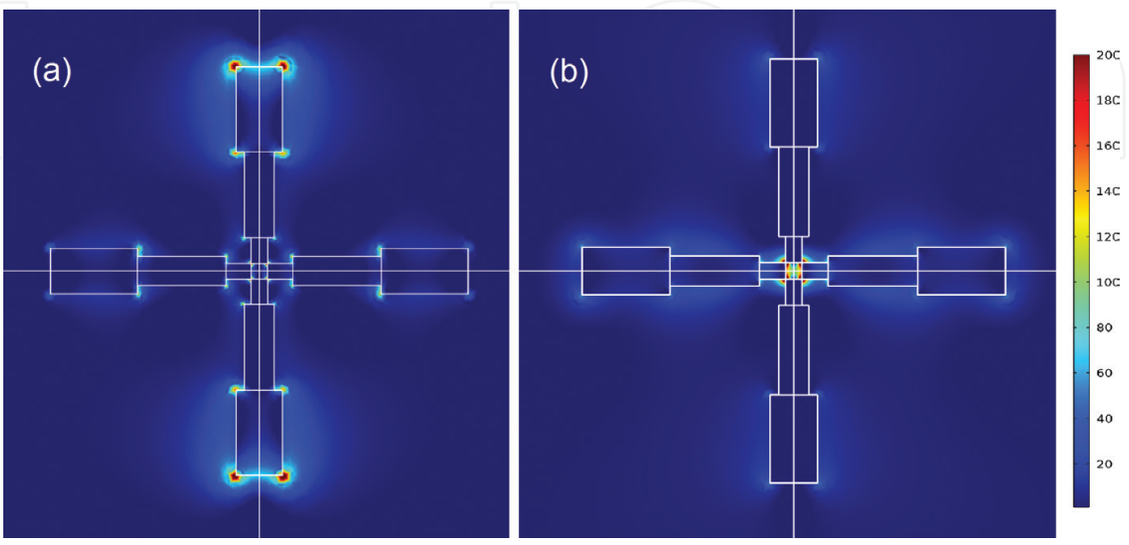

Figure 11. Electric field profile for the cross-tapered dipole nanoantenna at wavelengths of (a) 425 nm and (b) 530 nm.

Figures 12 and **13** show the variation of the harvesting efficiency and the resonance impedance with the studied parameters W_1 and L_1, respectively. Additionally, the summary of the tolerance study is listed in **Table 4**. It is evident from **Figures 12** and **13** and **Table 4** that the proposed design has a tolerance of ±5% at which the harvesting efficiency is still higher than 53.8% with a maximum deviation of ±58 Ω from the optimum input impedance of the nanoantenna. Additionally, a maximum wavelength resonance shift of 10 nm is obtained within the tolerance of ±5% of the studied parameters. Therefore, it is evident from the above results that the proposed nanoantenna design bears high robustness for fabrication imperfection.

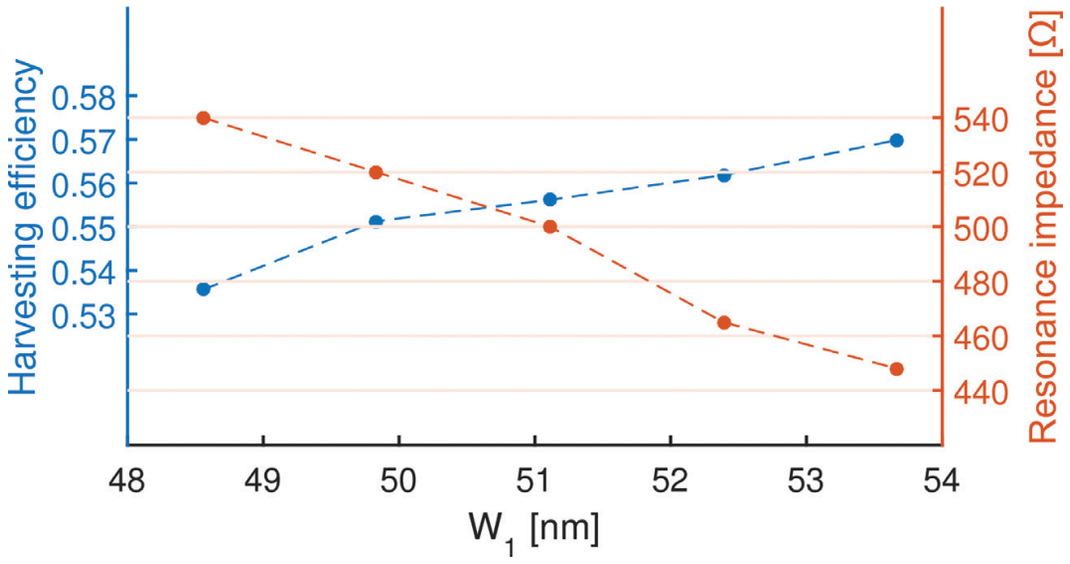

Figure 12. Values of harvesting efficiency and resonance impedance with 5% variation of W_1 parameter.

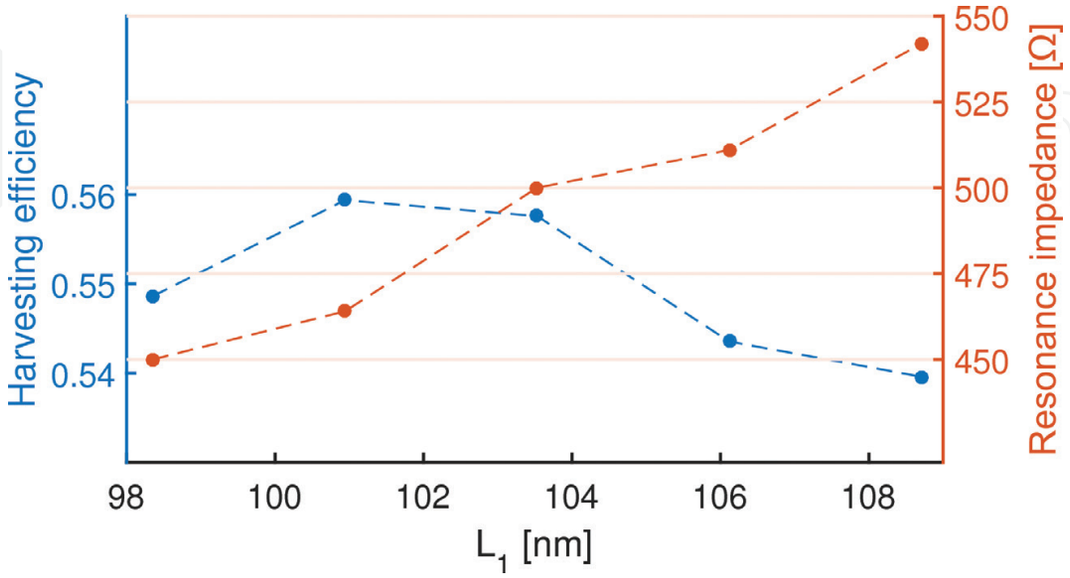

Figure 13. Values of harvesting efficiency and resonance impedance with 5% variation of L_1 parameter.

Parameter	Tolerance	Harvesting efficiency	Impedance
L_1	103.5 nm ± 5%	Higher than 53.9%	500 Ω ± 54 Ω
W_1	51 nm ± 5%	Higher than 53.8%	500 Ω ± 58 Ω
L_2	70 nm ± 5%	Higher than 55.2%	500 Ω ± 35 Ω
W_2	19.5 nm ± 5%	Higher than 55.25%	500 Ω ± 31 Ω
L_3	5 nm ± 5%	Higher than 55.45%	500 Ω ± 30 Ω
W_3	13.4 nm ± 5%	Higher than 55.5%	500 Ω ± 27 Ω

Table 4. Fabrication tolerance for tapered dipole design parameters [3] at λ = 500 nm.

6. Conclusion

In this chapter, a full study for novel-tapered nanoantenna designs have been implemented where antenna input impedance, return loss, harvesting efficiency, and field confinement were calculated using FEFD method. The simulation results show that the tapered design can achieve a harvesting efficiency of 60% at wavelength of 500 nm, which is higher than that of conventional dipole counterpart by 34%. Further, the antenna input impedance is tuned to match the impedance of fabricated diodes. Additionally, the cross-tapered-dipole nanoantenna achieved a near-field intensity enhancement of 252 V/m which is higher than previously reported symmetric cross nanoantenna. The spatial and spectral distinction of the resonance modes in the cross structure allows the cross-tapered-dipole to be utilized in color-sorting and fluorescence-sensing applications. Finally, the fabrication tolerance study shows that the proposed nanoantennas bear high robustness for fabrication imperfection.

Author details

Youssef Mamdouh El-Toukhy[1,2], Mohamed Farhat Othman Hameed[1,2], Mohamed Hussein[1,3] and Salah Sabry Ahmed Obayya[1,2]*

*Address all correspondence to: sobayya@zewailcity.edu.eg

1 Centre for Photonics and Smart Materials, Zewail City of Science and Technology, Giza, Egypt

2 Faculty of Engineering, Mansoura University, Mansoura, Egypt

3 Department of Physics, Faculty of Science, Ain Shams University, Cairo, Egypt

References

[1] D. K. Kotter, S. D. Novack, W. D. Slafer, and P. J. Pinhero, "Theory and manufacturing processes of solar nanoantenna electromagnetic collectors," *Journal of Solar Energy Engineering*, vol. 132, pp. 011014-011014, 2010.

[2] S. Obayya, N. Areed, M. F. O. Hameed, and M. Hussein, "Optical nano-antennas for energy harvesting," *Innovative Materials and Systems for Energy Harvesting Applications*, IGI, Italy, p. 26, 2015.

[3] Y. M. El-Toukhy, M. Hussein, M. F. O. Hameed, A. M. Heikal, M. M. Abd-Elrazzak, and S. S. A. Obayya, "Optimized tapered dipole nanoantenna as efficient energy harvester," *Optics Express*, vol. 24, pp. A1107-A1122, 2016.

[4] M. Hussein, N. F. F. Areed, M. F. O. Hameed, and S. S. A. Obayya, "Modified elliptical nanoantenna for energy harvesting applications," in *2016 IEEE/ACES International Conference on Wireless Information Technology and Systems (ICWITS) and Applied Computational Electromagnetics (ACES)*, 2016, pp. 1-2.

[5] F. B. Zarrabi, M. Naser-Moghadasi, S. Heydari, M. Maleki, and A. S. Arezomand, "Cross-slot nano-antenna with graphene coat for bio-sensing application," *Optics Communications*, vol. 371, pp. 34-39, 2016.

[6] N. Verellen, P. Van Dorpe, C. Huang, K. Lodewijks, G. A. E. Vandenbosch, L. Lagae, *et al.*, "Plasmon line shaping using nanocrosses for high sensitivity localized surface plasmon resonance sensing," *Nano Letters*, vol. 11, pp. 391-397, 2011.

[7] A. M. Ghanim, M. Hussein, M. F. O. Hameed, A. Yahia, and S. S. A. Obayya, "Highly directive hybrid Yagi-Uda nanoantenna for radiation emission enhancement," *IEEE Photonics Journal*, vol. 8, pp. 1-12, 2016.

[8] R. L. Bailey, "A proposed new concept for a solar-energy converter," *Journal of Engineering for Power*, vol. 94, pp. 73-77, 1972.

[9] S. Grover and G. Moddel, "Applicability of metal/insulator/metal (MIM) diodes to solar rectennas," *IEEE Journal of Photovoltaics*, vol. 1, pp. 78-83, 2011.

[10] G. A. E. Vandenbosch and Z. Ma, "Upper bounds for the solar energy harvesting efficiency of nano-antennas," *Nano Energy*, vol. 1, pp. 494-502, 2012.

[11] Z. Ma and G. A. E. Vandenbosch, "Optimal solar energy harvesting efficiency of nano-rectenna systems," *Solar Energy*, vol. 88, pp. 163-174, 2013.

[12] M. N. Gadalla, M. Abdel-Rahman, and A. Shamim, "Design, optimization and fabrication of a 28.3 THz nano-rectenna for infrared detection and rectification," *Scientific Reports*, vol. 4, p. 4270, 03/06/online 2014.

[13] H. Fischer and O. J. F. Martin, "Engineering the optical response of plasmonic nanoantennas," *Optics Express*, vol. 16, pp. 9144-9154, 2008.

[14] Z. Iluz and A. Boag, "Dual-Vivaldi wideband nanoantenna with high radiation efficiency over the infrared frequency band," *Optics Letters*, vol. 36, pp. 2773-2775, 2011.

[15] E. Briones, J. Alda, and F. J. González, "Conversion efficiency of broad-band rectennas for solar energy harvesting applications," *Optics Express*, vol. 21, pp. A412-A418, 2013.

[16] M. Hussein, N. F. Fahmy Areed, M. F. O. Hameed, and S. S. Obayya, "Design of flower-shaped dipole nano-antenna for energy harvesting," *Optoelectronics IET*, vol. 8, pp. 167-173, 2014.

[17] J. L. Stokes, Y. Yu, Z. H. Yuan, J. R. Pugh, M. Lopez-Garcia, N. Ahmad, *et al*., "Analysis and design of a cross dipole nanoantenna for fluorescence-sensing applications," *Journal of the Optical Society of America B*, vol. 31, pp. 302-310, 2014.

[18] E. Segal, A. Weissman, D. Gachet, and A. Salomon, "Hybridization between nanocavities for a polarimetric color sorter at the sub-micron scale," *Nanoscale*, vol. 8, pp. 15296-15302, 2016.

[19] Z. Zhang, A. Weber-Bargioni, S. W. Wu, S. Dhuey, S. Cabrini, and P. J. Schuck, "Manipulating nanoscale light fields with the asymmetric Bowtie nano-colorsorter," *Nano Letters*, vol. 9, pp. 4505-4509, 2009.

[20] Y. Ying-Ying, L. Qian-Guang, Y. Hai-Juan, and L. Xue-Chun, "The generation of MHz isolated XUV attosecond pulses by plasmonic enhancement in a tailored symmetric Ag cross nanoantenna with a few-cycle laser," *Laser Physics*, vol. 23, p. 045301, 2013.

[21] J. Kennedy and R. Eberhart, "Particle swarm optimization," in *IEEE International Conference on Neural Networks*, *1995*. *Proceedings*, 1995, pp. 1942-1948, vol. 4.

[22] F. F. K. Hussain, A. M. Heikal, M. F. O. Hameed, J. El-Azab, W. S. Abdelaziz, and S. S. A. Obayya, "Dispersion characteristics of asymmetric channel plasmon polariton waveguides," *IEEE Journal of Quantum Electronics*, vol. 50, pp. 474-482, 2014.

[23] C. Multiphysics®, 5.1, Ed., COMSOL AB, Stockholm, Sweden, 2016.

[24] W. Hu, K. Sarveswaran, M. Lieberman, and G. H. Bernstein, "Sub-10 nm electron beam lithography using cold development of poly(methylmethacrylate)," *Journal of Vacuum Science & Technology B*, vol. 22, pp. 1711-1716, 2004.

[25] J.-T. Lv, Y. Yan, W.-K. Zhang, Y.-H. Liu, Z.-Y. Jiang, and G.-Y. Si, "Plasmonic nanoantennae fabricated by focused Ion beam milling," *International Journal of Precision Engineering and Manufacturing*, vol. 16, pp. 851-855, 2015.

[26] L. Chih Jen, A. Thomas, and B. Alexey, "Fabrication of symmetric sub-5 nm nanopores using focused ion and electron beams," *Nanotechnology*, vol. 17, p. 3264, 2006.

[27] P. F. A. Alkemade and E. van Veldhoven, "Deposition, milling, and etching with a focused helium ion beam," in *Nanofabrication*: *Techniques and Principles*, M. Stepanova and S. Dew, Eds., Vienna: Springer Vienna, 2012, pp. 275-300.

[28] Y. M. El-Toukhy, A. M. Heikal, M. F. O. Hameed, M. M. Abd-Elrazzak, and S. S. A. Obayya, "Optimization of nanoantenna for solar energy harvesting based on particle swarm technique," in *2016 IEEE/ACES International Conference on Wireless Information Technology and Systems* (*ICWITS*) *and Applied Computational Electromagnetics* (*ACES*), 2016, pp. 1-2.

[29] N. Jin and Y. Rahmat-Samii, "Particle swarm optimization for antenna designs in engineering electromagnetics," *Journal of Artificial Evolution and Applications*, vol. 2008, 2008.

[30] S. Xu, Y. Rahmat-Samii, and D. Gies, "Shaped-reflector antenna designs using particle swarm optimization: An example of a direct-broadcast satellite antenna," *Microwave and Optical Technology Letters*, vol. 48, pp. 1341-1347, 2006.

[31] P. J. Angeline, “Evolutionary optimization versus particle swarm optimization: philosophy and performance differences," presented at the Proceedings of the 7th International Conference on Evolutionary Programming VII, 1998.

[32] J. Vesterstrom and R. Thomsen, "A comparative study of differential evolution, particle swarm optimization, and evolutionary algorithms on numerical benchmark problems," in *Proceedings of the 2004 Congress on Evolutionary Computation* (*IEEE Cat. No.04TH8753*), 2004, pp. 1980-1987, vol. 2.

[33] E. A. Soliman, M. O. Sallam, and G. A. E. Vandenbosch, "Plasmonic grid array of gold nanorods for point-to-point optical communications," *Journal of Lightwave Technology*, vol. 32, pp. 4898-4904, 2014.

[34] P. B. Johnson and R. W. Christy, "Optical constants of noble metals," *Physical Review B*, vol. 6, p. 4370, 1972.

[35] A. a. E. Alù, Nader, "Input impedance, nanocircuit loading, and radiation tuning of optical nanoantennas," *Physical Review Letters*, vol. 101, p. 4, Jul 2008.

[36] C. Y. Chin and C. F. Jou, "A slim horizontally polarized omnidirectional antenna based on turnstile slot dipole,," *Progress in Electromagnetics Research C*, vol. 50, pp. 75-85, 2014.

[37] E. D. Palik, *Handbook of Optical Constants of Solids*. Orlando: Academic Press, 1985.

[38] J.-J. Greffet and F. Marquier, “Impedance of a nanoantenna and a quantum emitter," in *Frontiers in Optics 2011/Laser Science XXVII*, San Jose, California, 2011, p. LWG4.

[39] G. W. Bryant, F. J. García de Abajo, and J. Aizpurua, "Mapping the plasmon resonances of metallic nanoantennas," *Nano Letters*, vol. 8, pp. 631-636, 2008.

[40] X. Ren, W. E. I. Sha, and W. C. H. Choy, "Tuning optical responses of metallic dipole nanoantenna using graphene," *Optics Express*, vol. 21, pp. 31824-31829, 2013.

[41] J. Chen and Z. Zhang, "Bowtie nanoantennas with symmetry breaking," *Journal of Nanophotonics*, vol. 9, pp. 093798-093798, 2014.